Expression of Chirality by Competing Nucleated Self-Assembly

Jeffrey Everts

February 16, 2010

Supervisors:

prof. dr. ir. Paul van der Schoot[1]
dr. ir. Anja Palmans[2]
MSc. Seda Cantekin[2]

[1]Theory of Polymers and Soft Matter Group
Department of Applied Physics
Eindhoven University of Technology

[2]Laboratory of Macromolecular and Organic Chemistry
Department of Chemical Engineering and Chemistry
Eindhoven University of Technology

Abstract

In this paper, we report a competing nucleated self-assembly model for use in the description of the expression of chirality in deuterated benzene-1,3,5-tricarboxamides (D-BTAs). These molecules form helical supramolecular polymers, which are inherently chiral objects. A preference for the formation of a right-handed or left-handed helix is observed if deuterium is used for the formation of a stereocenter. The type of helix depends on the absolute configuration of the chiral monomeric unit. The net helicity can be measured with CD spectroscopy, while the fraction of polymerized material can be measured by UV-VIS spectroscopy. The model discussed in this work is able to predict experimental data obtained from these methods in a dilute solution of D-BTAs in a limited temperature regime, if the data is normalized such that at low temperatures a net helicity of unity is obtained.

Contents

Preface **4**

1 Introduction **5**

1.1 The expression of chirality 5

1.2 Nucleated self-assembly 8

1.3 Deuterated benzene-1,3-5-tricarboxamides (D-BTAs) 11

1.4 General approach and report structure 14

2 Competing nucleated self-assembly model **15**

2.1 Theory 15

2.2 The effect of mass action on a equally co-operative two-component system . . 18

2.3 Analytical solutions by perturbing κ_{BA} 20

2.4 Temperature dependent behavior of competing nucleated self-assembly 22

2.5 Length distributions 24

3 Comparison with experiment and experimental results **26**

3.1 Comparison with experiments in dodecane 26

3.2 Self-assembly of D-BTA in heptane at low temperatures 28

4 Conclusions and outlook **30**

A Heat capacity of a single quantum harmonic oscillator **33**

B Numerical implementation of the model **34**

C Choice of reference volume **37**

D Supporting figures **38**

Bibliography **40**

Preface

This report is the final result of the theoretical part of an internship done at the department of Applied Physics and the department of Chemical Engineering and is intended to serve as a final project for both bachelor programmes. The project consisted of two parts: a theoretical part meant for physics, while the chemistry part is purely experimental. Although this report is the final result of the theoretical part, the experimental part is not meant to be seen separate from this. For this reason I have chosen to include the most relevant experimental results in the first and third chapter as an introduction, motivation and discussion for the construction of the model. All other experiments are included in the report for the chemistry part, which is written up in an article style.

Since this project is intended to be interdisciplinary, I tried to make this report as readable as possible for both physicists and chemists. For this reason, I have worked out some explicit steps within the derivations. One particular example is that I have put the derivation of the heat capacity of a quantum harmonic oscillator in the Appendix. People with some background in statistical mechanics may of course already be familiar with these calculations. For physicists, I have tried to omit extensive chemical nomenclature, where possible. Furthermore, some necessary chemical principles are outlined in the first chapter.

I hope that you as reader will enjoy reading this report, regardless if you are a physicist or a chemist.

Jeffrey Everts

Chapter 1

Introduction

1.1 The expression of chirality

Helical structures formed by self-assembly processes are observed much in nature. A well known example is DNA, the carrier of our genetic material. The most common form of this macromolecule is a double helix, consisting of two helical strands of nucleic acids associated by hydrogen bonds (cf. Figure 1.1(a)). As another example, many helical substructures can be observed in proteins, the so-called α-helix (cf. Figure 1.1(b) and 1.1(c)). We can also observe helical aggregation on a whole other length scale. An example is F-actin, a supramolecular helical polymer consisting of globular proteins called G-actin [1]. See also Figure 1.1(d) and 1.1(e).

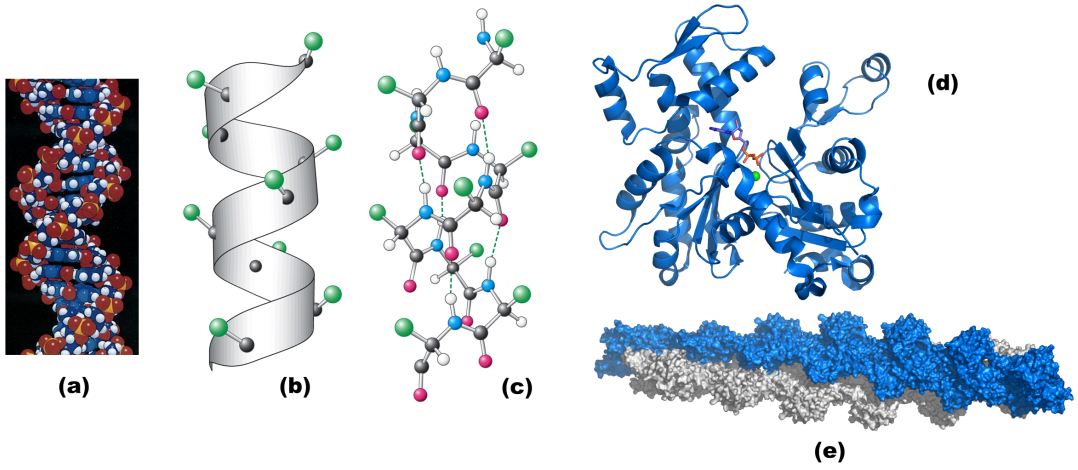

Figure 1.1: Various examples of helical architectures observed in living systems (a) DNA, a double helix that is formed by hydrogen bonds between complementary base pairs (taken from [1]). (b) A sequence of amino acids in an α-helical form. The helix is indicated by a ribbon (taken from [2]). (c) Part of the structure of the α-helix showing some chemical details (taken from [2]) (d) The tertiary structure of the protein G-actin. Notice the α-helices present in this structure (taken from Wikipedia). (e) The quaternary structure of F-actin, a helical supramolecular polymer consisting of G-actin (taken from Wikipedia).

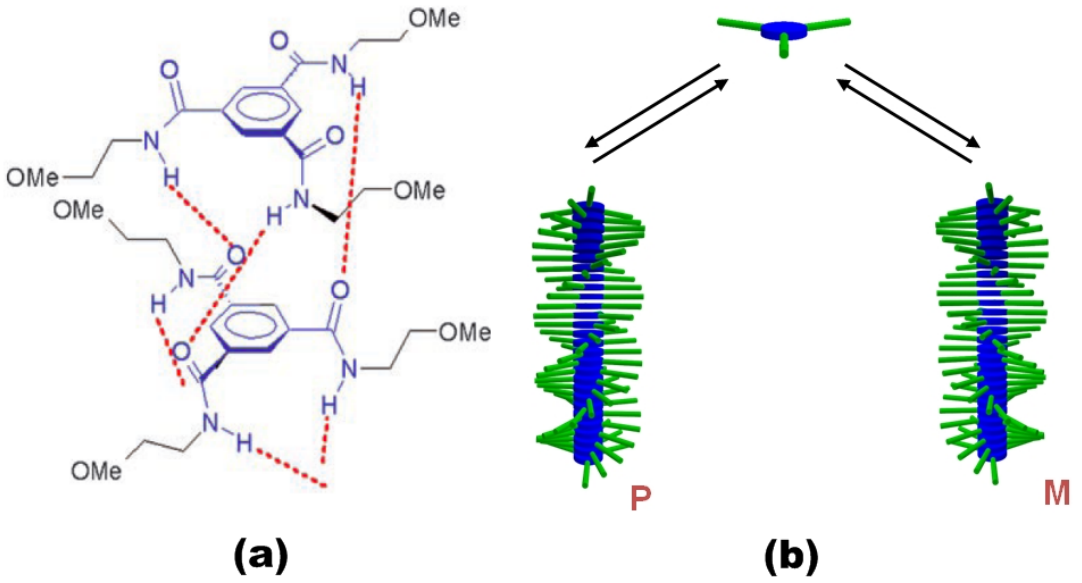

Figure 1.2: (a) Threefold intramolecular hydrogen bonding for a methoxyethyl functionalized BTA [3]. (b) Graphical representation for the helical self-assembly of a BTA in either a (*P*)- or (*M*)-helix. By introducing a stereocenter in the monomeric unit, the formation of one helix type is preferred.

Helices are chiral objects; it is an object that cannot be superimposed on its mirror image. Consequently, we can distinguish two types of helices: one that has a right handed orientation (or *P*-helix) and one that has a left-handed orientation (or *M*-helix). For a macromolecule with a helical conformation, a preference for one of the two helical senses is observed. For example, in DNA there is a preference for one of the two types of helices under certain external conditions (such as temperature, pH or salt concentration). We can distinguish many types of DNA conformations, but surprisingly a family of conformations that is most common in living cells (B-DNA), is right-handed [1]. The same holds for certain sequences of amino acids: due to restricted possibilities of bond orientations in the primary structure, certain aggregated states can be preferred. For example, there exist polypeptides for which a left-handed helix is the structure of preference [2]. The reason for the existence of this preference is not trivial. There are many mesoscopic interactions which contribute to the energetic state of the aggregate, and thus the structure of the aggregate.

The system that is considered in this project are benzene-1,3,5-tricarboxamides (BTAs), molecules that also self-assemble in helical structures. These are disc-like molecules (or discotics), consisting of a central benzene core, with three alkyl tails coupled by amide bonds to this central core. The general structure of an asymmetrical BTA can be found in Figure 1.3. This molecule is able to form threefold hydrogen bonds with other molecules of the same type, which accommodates the formation of a quasi one-dimensional, linear, helical supramolecular polymer. This was first observed by Lightfoot et al. for methoxyethyl functionalized BTAs in the solid state by X-ray diffraction studies (cf. Figure 1.2(a)) [3]. The formation of a BTA helix by threefold

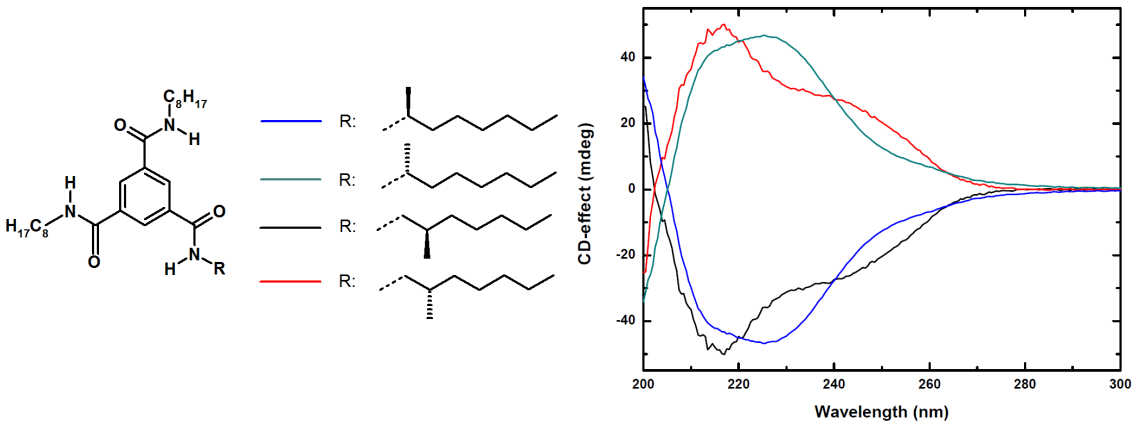

Figure 1.3: Expression of chirality for a solution of a methyl substituted BTA in methylcyclohexane ($3 \cdot 10^{-5}$M). For various residual groups the CD effect is shown. The CD effect is absent in an achiral molecule.

intermolecular hydrogen bonds is also observed in (dilute) solutions [4]. In general, if the monomeric units are achiral, equal amounts of P- and M-helices are formed. However, if we introduce a stereocenter in the monomers, it will result in a preference for the formation of one of the two helix types. Alternatively said for this case, chirality on a molecular, or microscopic scale is transferred to the mesoscopic scale of an aggregate. We will define this effect as *the expression of chirality* on the supramolecular scale. It is absent if we consider the same molecule without the stereocenter; equal amounts of P- and M-helices then exist. See also Figure 1.2(b). It is unknown why this effect is observed. Presumably, it is due to the confinement of space by the residual group that introduced the stereocenter, but we shall see in section 1.3 that this does not need to be the case.

A typical way to observe the bias of one type of helical aggregate, is by measuring the circular dichroism spectrum in (dilute) solutions [5]. Circular dichroism or CD is the difference in absorption between left- and righthanded circularly polarized light. This effect is expressed by a value called the CD effect (given in mdeg). Sometimes this quantity is corrected for concentration and the path length of the cuvette. We call this normalized value $\Delta\epsilon$ and it is defined as $\Delta\epsilon :=$ CD effect$/(32980 \cdot c \cdot l)$, with c the concentration in M and l the path length in cm. As a final remark, we note that circular dichroism measured in the vicinity of an absorption band of the substance is called a Cotton effect.

A preference for one type of helix (e.g. P-helix) results in a CD spectrum with a particularly shape that depends on the shape of the aggregate and the molecular architecture of the monomeric units [5]. An example is shown in Figure 1.3 from the work of Stals et al. [4] for various chiral methylated BTAs. As can be seen, these methyl substituted BTAs show a significant Cotton effect. The maximum amplitude of the CD effect is proportional to the net helicity, which is a measure for the preference of one type of helix over the other. Furthermore, notice that the CD spectra of two enantiomers are perfect mirror images of each other.

Another interesting feature of chiral methylated BTAs can be observed in Figure 1.3.

It is observed that the position of the methyl substituent in the aliphatic tail determines the shape and sign of the CD spectrum. Moreover, it depends on whether it is positioned on a odd or even position in the alkyl chain. This is called an odd-even effect in shape and sign of the CD spectrum. Stals et al. hypothesize that this effect is caused by steric hindrance of the methyl group in the helical aggregate, which is different for an odd or even position. This difference in steric interaction will result in a different helical packing or even a different helical sense. This is expressed in the two observed shapes of the CD spectra.

We hope to have shown that CD spectroscopy is an interesting technique to investigate systems, in which a net helicity can be observed. Often this technique is complemented with UV-VIS spectroscopy. Since the absorption spectrum of an aggregate differs from that of the molecularly dissolved state, the absorbance or optical dispersity (O.D.) is a measure for the fraction polymerized material. These techniques together are used to investigate the dependency of the system for various conditions such as concentration and temperature. The temperature dependence will be discussed in the next section.

1.2 Nucleated self-assembly

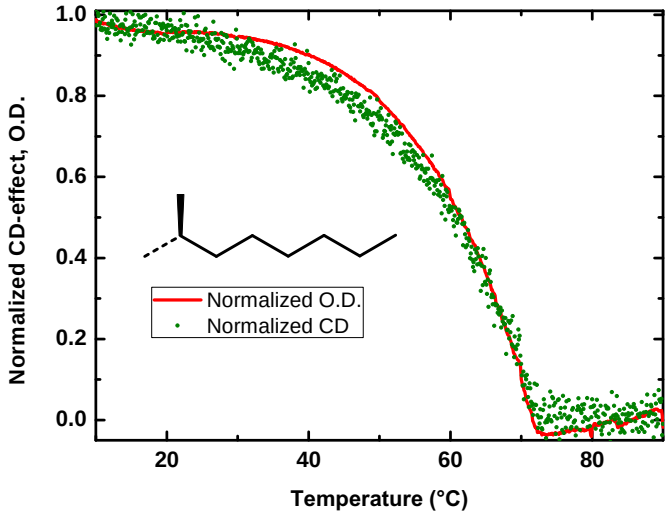

Figure 1.4: Nucleated self-assembly of a asymmetrical methylated BTA in a solution of $3 \cdot 10^{-5}$ M in dodecane, with the residual group shown in the graph. The fact that this process is co-operative is expressed in the sharp transition from the molecularly dissolved state to the polymerized regime. In this Figure the transition occurs at the polymerization temperature $T_p = 72°C$. Notice the similarity in shape of these cooling traces for the UV-VIS measurement and CD measurement.

As was already outlined in the previous section, CD and UV-VIS spectroscopy are useful techniques to investigate the self-assembly of BTAs in helical objects as a function of temperature. Usually, this is done by probing the CD effect or O.D. for various temperatures at a particular wavelength (usually the maximum absolute value of the

Cotton-effect). Since these values are proportional to the net helicity and fraction polymerized material, we can measure these quantities as function of temperature, if normalized in a correct manner. An advantage of these spectroscopic measurements is that they can be automated. In this way, many data points can be obtained for an accurate description of the process at hand. This is more difficult if we would like to do concentration dependent measurements. The disadvantage of this method is that it is not robust when the shape of the spectrum changes (e.g., when mixing two chromophores that have different Cotton effects). Care have to be taken in this case since we can only probe at one wavelength.

A typical cooling curve obtained with UV-VIS and CD spectroscopy is shown in Figure 1.4. In this example we have chosen a methylated BTA, that was also discussed earlier. There are many interesting and characteristic features concerning these kinds of curves. First of all, we can clearly distinguish between a regime in which all molecules are in solution (in this case at high temperatures) and a regime in which we have the polymerized state. This distinction is possible, since a free molecule does not exhibit a CD effect in solution at the given wavelength. This is not true with UV-VIS spectroscopy for the BTAs, since we measure an absorption spectrum in the molecularly dissolved state. Another issue is the absorption spectrum of the solvent. These effects combined result in a non-linear baseline for temperature dependent UV-VIS measurements. The resulting optical effects are seen in Figure 1.4 especially in the high temperature regime.

By using models, many useful information can be extracted from these UV-VIS and CD measurements. Different chemical models concerning the supramolecular polymerization exist (cf. Figure 1.5). Here we make a distinction between isodesmic self-assembly and nucleated self-assembly.

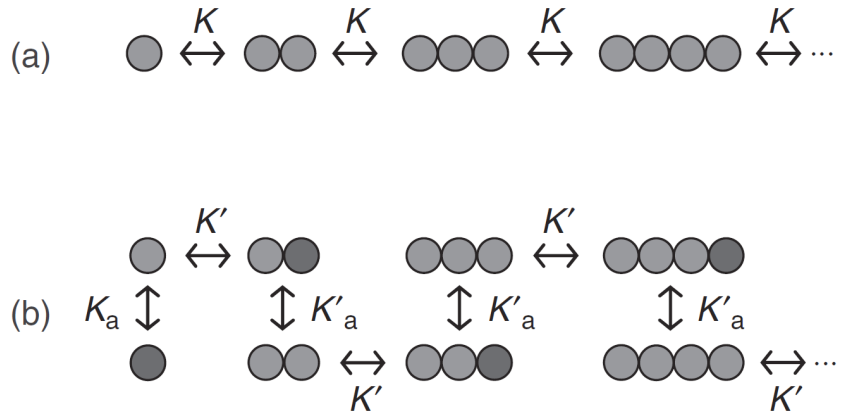

Figure 1.5: Different types of models for the self-assembly of supramolecular models. (a) Isodesmic self-assembly, the elongation constant K is assumed to be equal for all steps. (b) Nucleated self-assembly, in this type a monomeric unit can switch between an assembly active state and an assembly inactive state, governed by an activation constant $K_a << 1$ for monomeric units and K_a' for a monomeric unit in a growing polymer chain. We call the polymerization self-catalyzed or autosteric if $K_a' >> K_a$ (taken from [7]).

In the first case, the ease of an addition of a monomeric unit to a growing polymer chain is equal for all steps. For example, the equilibrium constant K for a monomer

to add to a trimer chain is equal as it would be for an addition to a pentamer chain. In the case of nucleated self-assembly, we discern the existence of an assembly active state and an assembly inactive state for the monomeric units. If the monomer is active, it can readily polymerize, if it is inactive it cannot. It reduces to the isodesmic case if the required energy to make the molecule active is very small. We call the polymerization nucleated or co-operative, if the transition form the inactive state to the activated state is very unfavorable. In this case, there exist a sharp transition that resembles a thermodynamic phase transition between the monomeric regime and the polymerized regime. Moreover, in the nucleated self-assembly model we can make a distinction between a self-catalyzed (or autosteric) process and a non self-catalyzed process. In the first case, the monomer needs to be activated prior to adding to the growing polymer chain, in every step of the polymerization process. In the latter case, there is no energy penalty if a monomer wants to bind to an existing aggregate of a certain length.

Both the self-catalyzed as the non self-catalyzed approach will lead to a mass action law. This is obtained by a free energy minimalization [8], [7] (see also Chapter 2). As usual, a mass action law is governed by a mass action variable $X := \phi K$, with K an equilibrium constant regulated by a free energy of binding g by $K := \exp(-\beta g)$. Chemists usually call this equilibrium constant an elongation constant (K_e). In this definition, ϕ indicates a mole or volume fraction. Together in the definition of the variable X, it says something about the a priori probability of a monomer actually attaching to a growing aggregate. In the case of non-autosteric nucleated self-assembly it will result in a mass action law of the following form,

$$XK_a = 1 - \overline{N}_a^{-1} + K_a(\overline{N}_a - 1)\overline{N}_a. \tag{1.1}$$

Here $K_a << 1$ is called the activation constant which acts as an equilibrium constant between the active state of a monomer and the inactive state. $\overline{N}_a$ is defined as the mean aggregation number of active species. In contrast, we find for the self-catalyzed form,

$$X = 1 - \overline{N}_a^{-1} + K_a(\overline{N}_a - 1)\overline{N}_a. \tag{1.2}$$

As is seen, these two equations can be interchanged by a redefinition of the mass action variable. In practice, this means that you cannot distinguish autosteric and non-autosteric self-assembly by using this method. To do this, we need kinetic measurements.

This mass action law can be used to derive an approximate expression for the fraction polymerized material η,

$$\eta \sim 1 - \exp\left(\frac{-h_p}{k_B T_p}\left(\frac{T}{T_p} - 1\right)\right). \tag{1.3}$$

Here h_p is the enthalpy of elongation as defined on the polymerization temperature T_p and as usual k_B is the Boltzmann constant. Outside the polymerized regime,

$\eta = 0$. Near the polymerization temperature we can find a more accurate expression if $K_a << 1$, given by,

$$\eta \sim K_a^{\frac{1}{3}} \exp\left(\frac{2}{3} K_a^{-1/3} h_p (T/T_p - 1)/k_B T_p\right). \tag{1.4}$$

This model is in fact a simplification of the actin polymerization model of Oosawa and Kasai [6] and we can fit experimental data by using equations 1.3, 1.4. This model will give us information about the co-operativity of the system (K_a) (i.e., the sharpness of the transition between the molecularly dissolved regime and polymerized regime). The value of this constant is smaller if the self-assembly is co-operative. Furthermore, it gives information about the enthalpy release on elongation (i.e., the growth) of the polymer chain by h_p. Notice that prior to fitting, the data need to be normalized. This normalization is usually done arbitrarily by taking the largest CD effect or O.D.. We then assume that at that point a situation is achieved in which all monomeric units are in an aggregated state of only one helical screw sense. This is called a homochiral state. It is also common to fit the CD cooling curve as if it is a measure for the fraction polymerized material. This procedure is motivated by the similar shape of CD and UV-VIS cooling curves for most chiral BTAs. We then assume that only one type of helix is formed exclusively in the polymerized regime.

1.3 Deuterated benzene-1,3-5-tricarboxamides (D-BTAs)

In the case of methylated BTAs, the residual groups that introduce the stereocenters were large enough to offer a significant amount of steric hindrance in an aggregate. It is interesting to see the effect of making this residual group much smaller to the very limits of molecular chirality. The smallest stereocenter that we could introduce is simply by replacing a hydrogen atom by a deuterium[1]. The difference between a hydrogen atom and a deuterium is very small (only one neutron), so we do not exaggerate if we say that such a molecule is on the borderline of being chiral or achiral. The stereocenter that is formed in this way, is very small as compared to a large group such as a methyl on the electronic level. The real difference is present on the vibrational level, as is reflected in the different vibrational energies of a C-H bond compared to a C-D bond. We can imagine that the preference for one type of helix will not be that pronounced for such a system.

It is shown by Green et al. that indeed a deuteration results in the expression of chirality [9]. However, this work was done on polyisocyanates, a covalent polymer, but not for a supramolecular polymer. Inspired by this work, the two enantiomers of a symmetric deuterated BTA (D-BTA) were synthesized by Dirk Balkenende and Seda Cantekin, and chirality is indeed expressed at a supramolecular level for this system [10]. As expected, the temperature dependency of the CD effect is much weaker than

[1] Actually the smallest possible stereocenter known is by bringing a certain part of the molecule in an excited state.

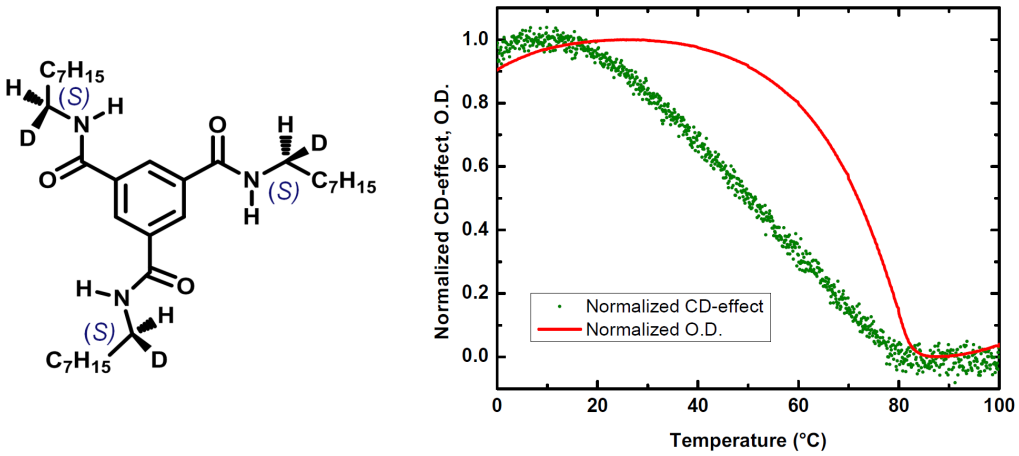

Figure 1.6: Cooling curves as obtained in CD and UV-VIS spectroscopy at $\lambda = 223$ nm at a concentration of $5 \cdot 10^{-5}$ M in dodecane. The data has been normalized in order to give a good comparison between the two cooling traces. In the left Figure the structural formula of the (S)-enantiomer of the D-BTA is shown. Experimental data is taken from [10].

for the methylated BTAs. In contrast, the shape of the curve measured with UV-VIS as a function of temperature *is* similar to that of the methylated BTAs. (cf. Figure 1.6). These effects together cannot be predicted by the nucleated self-assembly model as described in the previous section.

Moreover, a Cotton effect was only observed if linear alkanes were used as a solvent (e.g., heptane and dodecane). In branched or cyclic alkanes, such as respectively iso-octane and methylcyclohexane (MCH), the effect was completely absent (cf. Figure 1.7(a)).

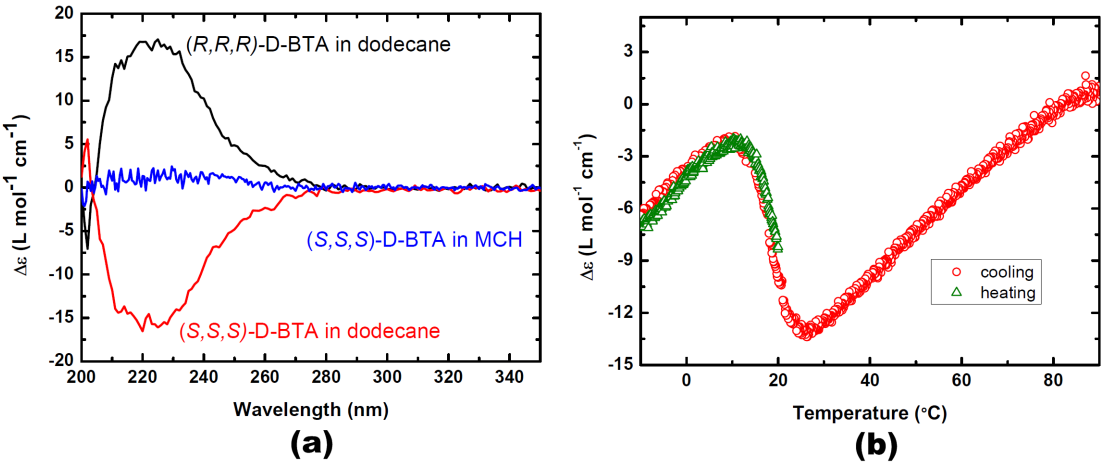

Figure 1.7: (a) Cotton effects at room temperature for D-BTAs in various solvents at $c = 5 \cdot 10^{-5}$ M . (b) Temperature dependent CD data as monitored at 223 nm for a D-BTA solution in heptane ($c = 5 \cdot 10^{-5}$ M). The sample was heated after the first cooling run, to investigate the presence of hysteresis. No significant hysteresis was observed. Also note that the data is not normalized.

These two results motivate us to believe that indeed not all the aggregates are present in just one helix orientation. We can hypothesize that there is a competition between the formation of P-type helices and M-type helices, as expressed in a difference between the CD and UV-VIS cooling curves. The equilibrium between these two species, is shifted to one side if a linear alkane is used as a solvent. If we would consider a solution in a cyclic or branched alkane, there is no preference for one of the two species. We then have equal amounts of P-type helices and M-type helices, and consequently a zero net helicity. As a remark, we note that a competition between two kinds of supramolecular polymer was also observed in bis-urea compounds by Bouteiller et al. [11].

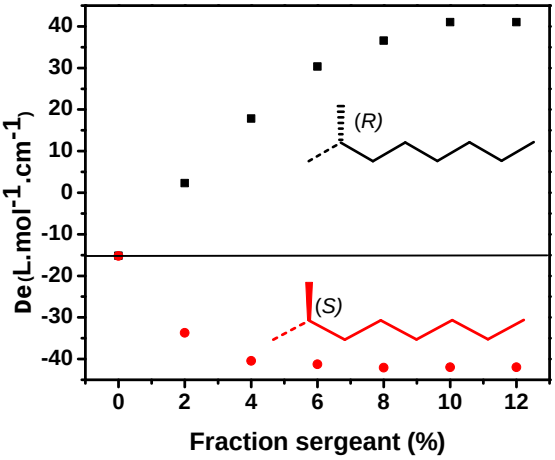

Figure 1.8: Sergeant added to a solution of (S)-D-BTA in dodecane. Two enantiomers of a methylated BTA were used as a sergeant, with the side chains shown in the figure. 6% sergeant was needed to bias the D-BTA to a preferred helix type, while 10% was needed to bias it to the other type. Experimental data taken from [10].

Interestingly, if we look at temperature dependent CD in heptane and let the temperature vary between $-10°$C and 90°C, we observe two extrema in the low temperature regime (Figure 1.7(b)). These extrema are reproducible even if the sample is heated after cooling (Figure 1.7(b)). Furthermore, these effects are not seen in UV-VIS (Figure D.1). These extrema may also be present for a solution in dodecane, but we are then not able to measure this, since the sample cannot cooled down to sufficient low temperatures. This is due to the high melting point of dodecane ($-9.6°$C). We believe that the presence of these extrema cannot be explained by the competition hypothesis followed earlier. We therefore hope to predict the net helicity as function of temperature only for a limited temperature regime. In the case of the measurements in heptane, this would be the regime from 20°C to 90°C. A discussion of these extrema is found in section 3.2.

We conclude this section with an experiment in which a Sergeant-and-Soldiers (SaS) like effect is used. The SaS-effect is observed if we add small amounts of a chiral molecule (the sergeant) to a solution of achiral molecules (the soldiers). All the achiral molecules are then biased to the helical screw sense of the chiral "seed". A similar effect can be realized, if we add a chiral BTA that has superimposable CD and UV-VIS

curves as function of temperature, indicating that this system has a more pronounced preference for a certain type of helix. This experiment is done by Seda Cantekin [10] by titrating a chiral methylated BTA to a D-BTA solution and the result is shown in Figure 1.8.

We observe in this experiment that adding a stronger sergeant results in an increase of the CD effect (in absolute value). This experiment shows that we need to take care when normalizing the experimental results, since it makes the choice of data normalization very difficult (and this could even be so in the case of methylated BTAs). From these experiments, we can hypothesize that the D-BTA system saturates at a net helicity of 0.35.

1.4 General approach and report structure

The interesting features of D-BTAs as described in the previous section motivate us for having a closer look to these systems. In this report we will discuss a procedure to describe nucleated self-assembly in the case of two competing species by extending the Oosawa and Kasai model for nucleated self-assembly. The construction of this model will be much similar to the approach of the one-component model as discussed in section 1.2. With this approach, we hope to describe the net helicity and fraction polymerized material as a function of temperature in a limited temperature regime. For this purpose, the dodecane measurements will be used for testing the model.

The model will be derived in Chapter 2 and we will see that it will result in a mass action law much similar to the one component model. Then we will use perturbation theory in order to obtain analytical solutions for a system in which the preference for the formation of one helix type over the other is small. As a final result, we will use the model to calculate length distributions of the different types of aggregate. In Chapter 3, we try to fit the experimental data by simulation. We will also discuss some experimental results that are done within this project and which are relevant for the discussion of the model. For details about these experiments, we refer to [12].

Chapter 2

Competing nucleated self-assembly model

2.1 Theory

In this section we will set up the general equations that we will use in our model to describe the co-operative self-assembly of discotics in helical aggregates. For this purpose a non-selfcatalyzed model is made, in which we will consider the existence of inactive species i, and active species A and B. A could be for instance a P-helix, while obviously B would then be a M-helix or vice versa. Within a saddle point approximation, we can write the free energies as follows.

The free energy for the inactive species i is,

$$\frac{\beta f_i}{V} = \rho_i \ln(\rho_i \upsilon) - \rho_i - \rho_i \ln Z_i, \tag{2.1}$$

while for the active species $\alpha = A,B$ the free energy is given by the expression,

$$\frac{\beta f_\alpha}{V} = \sum_{N=1}^{\infty} \rho_\alpha(N)[\ln(\rho_\alpha(N)\upsilon) - 1 - N \ln Z_\alpha + \beta G_\alpha(N-1)]. \tag{2.2}$$

The total free energy is then given by,

$$f = f_i + \sum_\alpha f_\alpha. \tag{2.3}$$

Here β is as usual the reciprocal of thermal energy given by $\beta := \frac{1}{k_B T}$ with k_B the Boltzmann constant and T the absolute temperature, V is the system volume, υ is the volume of a solvent molecule, ρ_k with k=i, A, B is the number density of species k, Z_k is the partition function for a monomer of species k, and finally G_α is a free energy of binding for the formation of an aggregate. Note that in 2.2, the first two terms between brackets [...] are an ideal mixing entropy term, while the third and last term are respectively from the free energy contributions of the monomers and of the aggregates.

Furthermore, we have the conservation of mass:

$$\phi_i = \rho_i \upsilon, \tag{2.4}$$

$$\phi_\alpha = \sum_{N=1}^{\infty} N \rho_\alpha(N) \upsilon, \tag{2.5}$$

$$\phi = \phi_i + \sum_{\alpha=A,B} \phi_\alpha. \tag{2.6}$$

Here ϕ denotes a mole fraction, since we have used for our definition of υ the volume of a solvent molecule (see Appendix C). Note also the definition of the mole fraction of active species 2.5. Here we correct for the length of the aggregate N, to make sure that ϕ is a conserved quantity.

We can find the optimal distributions by means of a functional minimalization of the free energy with respect to the various number densities by: $\frac{\delta f}{\delta \rho_k} = 0$, under the constraint of mass conservation. The optimal distributions for the inactive species are then given by,

$$\phi_i = \exp(\beta\mu) Z_i =: \lambda, \tag{2.7}$$

with λ the fugacity. Furthermore, we can use this definition of fugacity to show that we can find for the number density for species α of length N by,

$$\rho_\alpha(N)\upsilon = \Lambda_\alpha^N \exp(\beta G_\alpha), \tag{2.8}$$

where we have used the definition $\Lambda_\alpha := \lambda \exp(-\beta G_\alpha) \frac{Z_\alpha}{Z_i}$. Using this result, we can also find an expression for the number density of species α,

$$\upsilon \rho_\alpha := \sum_{N=1}^{\infty} \rho_\alpha(N)\upsilon = \exp(\beta G_\alpha) \frac{\Lambda_\alpha}{1-\Lambda_\alpha}. \tag{2.9}$$

And we can do the same for the mole fraction of species α,

$$\phi_\alpha := \sum_{N=1}^{\infty} N \rho_\alpha(N)\upsilon = \exp(\beta G_\alpha) \frac{\Lambda_\alpha}{(1-\Lambda_\alpha)^2}. \tag{2.10}$$

By using (2.9) and (2.10), we can determine the mean aggregation number of active species by the known recipe,

$$\overline{N}_\alpha = \frac{\phi_\alpha}{\rho_\alpha \upsilon} = \frac{1}{1-\Lambda_\alpha} \Leftrightarrow \Lambda_\alpha = 1 - \frac{1}{\overline{N}_\alpha}. \tag{2.11}$$

Using this expression in the definition for the mole fraction of species α (2.10), we find,

$$\phi_\alpha = \exp(\beta G_\alpha) \left(1 - \frac{1}{\overline{N}_\alpha}\right) \overline{N}_\alpha^2. \tag{2.12}$$

We now have the right tools to write the expression of the total mole fraction (2.6) of all species more explicitly,

$$\phi = \lambda + \sum_{\alpha} \exp(\beta G_\alpha) \frac{\Lambda_\alpha}{(1-\Lambda_\alpha)^2} \overset{*}{=} \Lambda_A \exp(\beta G_\alpha) \frac{Z_i}{Z_A} + \sum_{\alpha} \exp(\beta G_\alpha) \frac{\Lambda_\alpha}{(1-\Lambda_\alpha)^2}. \tag{2.13}$$

Here we have have taken at (*) $\alpha = A$ as our reference point for λ. By rewriting and subsequently working out (2.13), we find,

$$\phi K = 1 - \frac{1}{\overline{N}_A} + \frac{Z_A}{Z_i} \overline{N}_A (\overline{N}_A - 1) + \frac{Z_A}{Z_i} \exp(\beta(G_A - G_B)) \overline{N}_B^2 (1 - \frac{1}{\overline{N}_B}). \tag{2.14}$$

We have defined the dimensionless equilibrium constant K as the product of the activation constant of species A: (Z_A/Z_i), with the elongation constant of species A: $K_{e,\alpha} := \exp(-\beta G_\alpha)$. We can further simplify this expression by using (2.8) and (2.11) to establish a relation between species A and B,

$$1 - \frac{1}{\overline{N}_B} = \kappa_{BA} \left(1 - \frac{1}{\overline{N}_A} \right). \tag{2.15}$$

With $\kappa_{BA} := \frac{Z_B}{Z_A} \exp(\beta(G_A - G_B))$ a ratio of equilibrium constants. By using (2.15) in (2.14) and notice that we can only do this substitution for $\kappa_{BA} \neq 0$, we find,

$$\phi K = \underbrace{1 - \frac{1}{\overline{N}_A}}_{\text{monomers}} + \underbrace{\frac{Z_A}{Z_i} \overline{N}_A (\overline{N}_A - 1)}_{\text{polymers type A}} + \underbrace{\frac{Z_B}{Z_i} \frac{\overline{N}_B^2}{\overline{N}_A^2} \overline{N}_A (\overline{N}_A - 1)}_{\text{polymers type B}} \qquad (\kappa_{BA} > 0). \tag{2.16}$$

While for $\kappa_{BA} = 0$, we can find the following expression,

$$\phi K = 1 - \frac{1}{\overline{N}_A} + \frac{Z_A}{Z_i} \overline{N}_A (\overline{N}_A - 1) \qquad (\kappa_{BA} = 0). \tag{2.17}$$

Furthermore, we can find an inequality that holds for the ratio of aggregation numbers by means of (2.15),

$$\frac{\overline{N}_A}{\overline{N}_B} = \overline{N}_{\mathrm{A}} - \kappa_{BA} (\overline{N}_A - 1) \geq 0. \tag{2.18}$$

A consequence of this inequality is that we have to take care by doing a parametrization in $\overline{N}_A$, if B is preferred at certain conditions. The ratio of elongation constants can never be larger than one, if aggregates of species A are very large close to the long chain limit.

These calculations show us that we can find a mass action law for the formation of two helical aggregates, for which the mass action can be ascribed to the variable $X := \phi K$. As usual, the mass action variable X is the product of the a priori probability ϕ of a molecule being near the growing assembly and the enhancement K of this probability by the gain of free energy by actually attaching to it. Furthermore, we observe that this approach will lead to the law of mass action for one component (2.17), as it should be.

2.2 The effect of mass action on a equally co-operative two-component system

The quantity κ_{BA} in the previous section can be identified as a ratio of equilibrium constants and is a measure of the preference for the formation of species B over A. If we choose this quantity equal to unity, it directly means that the formation of both species is equally energetically favorable. In this section, we will investigate what happens if $\kappa_{BA} = 1$. According to our hypothesis, we have to find zero net helicity if we have a system that satisfies these conditions. This is the case if the formation of both species are equally co-operative, as we shall see next. Finally, we will investigate the influence of mass action on the fraction polymerized material and net helicity.

To work out these calculations, we assume that at the polymerization point the polymers are already very long, i.e. $\overline{N}_A >> 1$ if $\frac{Z_A}{Z_i} << 1$. By these assumptions, we observe that for $\kappa_{BA} = 1$, the aggregation numbers of species A and B are equal: $\overline{N}_B = \overline{N}_A$ The mass action is then given by,

$$\phi K = 1 + \overline{N}_A^2 \left(\frac{Z_A}{Z_i} + \frac{Z_B}{Z_i} \right). \tag{2.19}$$

For the net helicity we then find,

$$\langle \theta \rangle = \frac{\phi_A - \phi_B}{\phi_i + \sum_\alpha \phi_\alpha} = \frac{\overline{N}_A^2 (Z_A - Z_B)}{Z_i + \overline{N}_A^2 (Z_A + Z_B)} \tag{2.20}$$

We have chosen for this particular definition of the net helicity, since the CD effect is assumed to be proportional to the net helicity. Since $\phi := \phi_i + \sum_{\alpha=A,B} \phi_\alpha$ is a conserved quantity, we satisfy these experimental constraints. Moreover, we can identify Z_B/Z_i and Z_A/Z_i as the activation constants for respectively species A and B. As was mentioned earlier, we demand that in this case the net helicity is zero. This condition will be satisfied if $Z_B = Z_A$, or in other words: the growth of species A and B is equally co-operative. A direct consequence of this fact is that the quantity κ_{BA} can be interpreted as a ratio of elongation constants as in, $K_{e,B}/K_{e,A}$.

We can of course also calculate the fraction polymerized material by,

$$\eta := \frac{\sum_\alpha \phi_\alpha}{\phi_i + \sum_\alpha \phi_\alpha} = \frac{2K_a \overline{N}_A^2}{1 + 2K_a \overline{N}_A^2}. \tag{2.21}$$

Here we have made the observation that $K_a := \frac{Z_A}{Z_i} (= \frac{Z_B}{Z_i})$, and used again the fact that in this case $\overline{N}_B = \overline{N}_A$.

For an equally co-operative system the net helicity and fraction polymerized material are plotted as function of the mass action variable X. The plots are obtained by a parametrization with $\overline{N}_A$ and plotted for various values of κ_{BA}. We see that only small values of κ_{BA} are needed to have a significant effect. In Figure 2.1, the effect of the ratio of elongation constants is shown, while in Figure 2.2 the influence of co-operativity is emphasized.

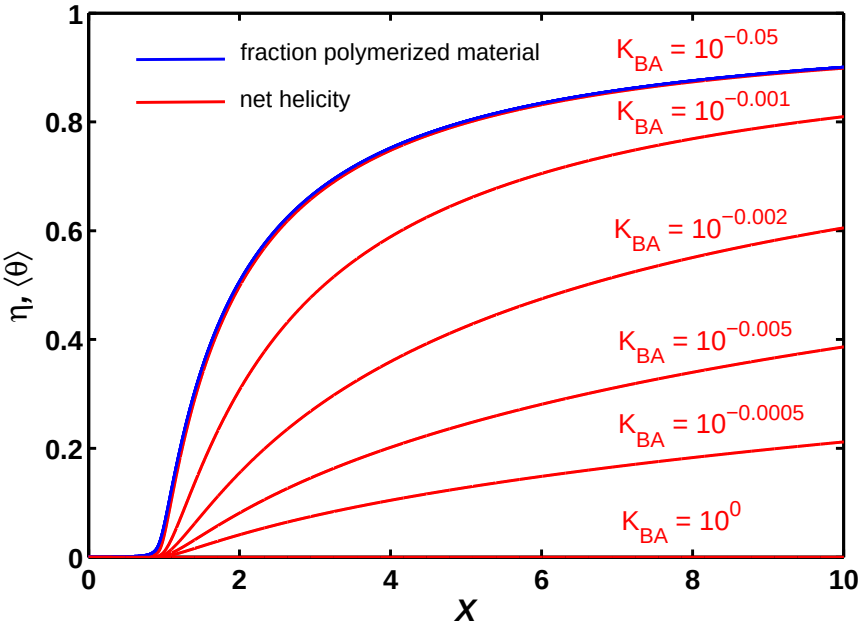

Figure 2.1: The dependence of the fraction polymerized material η and net helicity $\langle\theta\rangle$ as function of the mass action variable X for activation constant $K_a = 10^{-4}$. The dependence on the ratio of elongation constants κ_{BA} is shown, which is a measure of the preference of species B over A (where A is the preferred species in this case). As can be seen η is independent of this parameter and only small differences from $\kappa_{BA} = 1$ are needed such that η is superimposable on $\langle\theta\rangle$ as function of X.

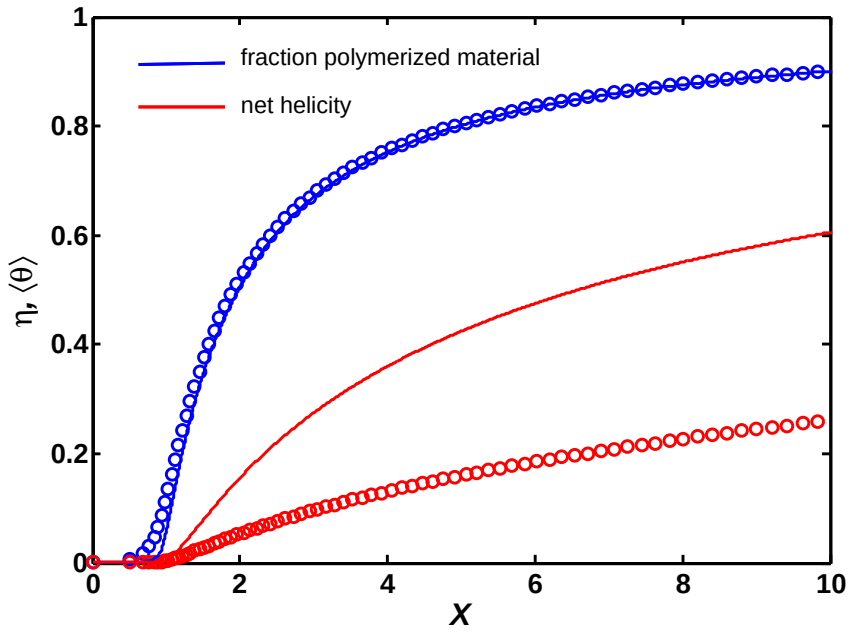

Figure 2.2: The dependence of the fraction polymerized material and net helicity as function of the mass action variable X for $\kappa_{BA} = 10^{-0.002}$. Here we show the influence of co-operativity on these quantities. The graphs of "$\circ$" corresponds to $K_a = 10^{-3}$, while the straight line "-" graphs correspond to $K_a = 10^{-4}$.

We conclude this section by constructing a similar scheme for the competing nucleated self-assembly model as in Figure 1.5. In this case every inactive species is activated as governed by an activation constant K_a. This is followed by growth in two possible types of aggregates labeled A and B. The growth of these aggregates are governed by equilibrium constants $K_{e,A}$ for active species A and $K_{e,B}$ for active species B. This scheme is given in Figure 2.3. Also notice the non self-catalyzed nature of this model and recall that the predictions for thermodynamic equilibria of this type of model are the same as that of a self-catalyzed version (section 1.2).

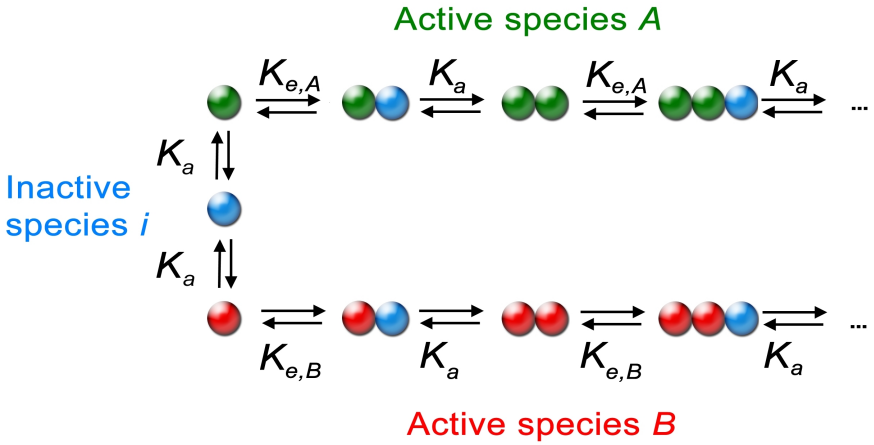

Figure 2.3: Chemical model for competing nucleated self-assembly. Every monomeric unit needs to be activated, as is expressed in an activation constant K_a, which is equal for both types of active species. The aggregates can grow after activation of a monomeric unit and these equilibria are established by elongation constants $K_{e,A}$ and $K_{e,B}$.

2.3 Analytical solutions by perturbing κ_{BA}

In this section, we will investigate the influence of a small preference for the formation of one active species over the other. This approach is justified since we saw in section 2.2 that only a small deviation from $\kappa_{BA} = 1$ is enough to give a significant effect. By doing this, we are able to derive analytical solutions for the net helicity $\langle\theta\rangle$ and for the fraction polymerized material η as a function of temperature. For this purpose, we will consider $\kappa_{BA} = 1 - \delta$ with $\delta > 0$ small. The choice for the positivity of δ is made to make sure that no problems arise due to the parametrization with $\overline{N}_A$. Furthermore, we again assume that starting from the polymerization point, the chains are already long (i.e., $\overline{N}_A >> 1$ for $K_a << 1$). The mass action can then be written as,

$$\phi K = 1 + K_a \overline{N}_A^2 \left(1 + \frac{\overline{N}_B^2}{\overline{N}_A^2} \right). \tag{2.22}$$

We can relate the aggregation number of species B to the aggregation number of species A, according to,

$$\frac{\overline{N}_B}{\overline{N}_A} = \frac{1}{\overline{N}_A - \kappa_{BA}(\overline{N}_A - 1)} = \frac{1}{\overline{N}_A(1-\kappa_{BA}) + \kappa_{BA}}. \tag{2.23}$$

Then rewriting (2.22) using the relation between the aggregation numbers (2.23) and by using the definition of the equilibrium constant K, we can write,

$$Y := (\phi K - 1)K_a^{-1} = \overline{N}_A^2 \left(1 + \frac{\overline{N}_B^2}{\overline{N}_A^2}\right). \tag{2.24}$$

Now we take $\kappa_{BA} = 1 - \delta$, then: $\overline{N}_A/\overline{N}_B = 1 + \overline{N}_A\delta$, such that,

$$X := \delta^2 Y = \delta^2 \overline{N}_A^2 (1 + (1 + \delta\overline{N}_A)^{-2}).$$

By defining $t := \delta\overline{N}_A$ and rewriting we find,

$$X(t+1)^2 = t^2((t+1)^2 + 1). \tag{2.25}$$

Now we consider three cases: (i) $t >> 1$, (ii) $t \simeq 1$ and (iii) $t << 1$,

(i) $t >> 1$: For this case, we find: $X \sim t^2$, or $\delta^2 Y \sim \delta^2 \overline{N}_A^2$, and thus: $Y \sim \overline{N}_A^2$;

(ii) $t \approx 1$: For this case, we find: $X = \frac{5}{4}t^2$, or $\delta^2 Y \sim \frac{5}{4}\delta^2 \overline{N}_A^2$, and thus: $Y \sim \frac{5}{4}\overline{N}_A^2$;

(iii) $t << 1$: For this case, we find: $X = 2t^2$, or $\delta^2 Y \sim 2\delta^2 \overline{N}_A^2$, and thus: $Y \sim 2\overline{N}_A^2$.

In all three cases, it can be seen that Y scales like $\overline{N}_A^2$ and thus $\overline{N}_A = \sqrt{Y}$. For $\phi K > 1$, the ratio of aggregation numbers is then given by: $\overline{N}_A/\overline{N}_B = 1 + \sqrt{Y}\delta$. Using all these expression, we find for the net helicity for small perturbations δ,

$$\langle\theta\rangle := \frac{\phi_A - \phi_B}{\phi_i + \sum_\alpha \phi_\alpha} = \frac{2\sqrt{Y}\delta K_a Y}{1 + 2\sqrt{Y}\delta + (2 + 2\sqrt{Y}\delta)K_a Y}. \tag{2.26}$$

While for the fraction polymerized material, we find,

$$\eta := \frac{\sum_\alpha \phi_\alpha}{\phi_i + \sum_\alpha \phi_\alpha} = \frac{(2 + 2\sqrt{Y}\delta)K_a Y}{1 + 2\sqrt{Y}\delta + (2 + 2\sqrt{Y}\delta)K_a Y}. \tag{2.27}$$

We have now shown that we are able to obtain closed form expressions for $\langle\theta\rangle$ and η. Later, we will discuss this result compared to solutions that are obtained numerically (Appendix B). Before we can do this, we have to introduce temperature dependency for these expressions. This will be done in the next section.

2.4 Temperature dependent behavior of competing nucleated self-assembly

Using the results of the previous section, we are able to write everything in a experimental more useful form by considering the fraction polymerized material and the net helicity as a function of temperature. First, we identify the quantity δ in terms of free energy. By definition of κ_{BA} and by resummation of the quantity δ (i.e., $1-\delta \sim \exp(-\delta)$), we find,

$$\delta \sim \beta(G_B - G_A). \tag{2.28}$$

Next, we can do a formal expansion around a certain reference temperature T^* for the free energies in the definition of δ and for the various equilibrium constants in the definition of Y. In general any equilibrium constant can be written as $K = \exp(-\beta g)$ with g a free energy of binding of a single monomer. Expanding $-\beta g$ up until second order, we find,

$$\begin{aligned} -\beta g &= -\beta g\Big|_{T=T^*} - \left(\frac{\partial \beta g}{\partial T}\right)\Big|_{T=T^*}(T-T^*) - \frac{1}{2}\left(\frac{\partial^2 \beta g}{\partial T^2}\right)\Big|_{T=T^*}(T-T^*)^2 + ... \\ &= \ln K^* + \frac{h^*}{k_B T^*}\left(\frac{T}{T^*}-1\right) + \frac{C_p^* T^* - 2h^*}{2k_B T^*}\left(\frac{T}{T^*}-1\right)^2 + ... \quad . \end{aligned} \tag{2.29}$$

Every quantity marked with a asterisk indicates that the value is defined at the reference temperature T^*. We are free to choose this reference temperature to be the polymerization temperature T_p, such that $\phi K_a^* K_{e,A}^* = 1$. Furthermore, we choose to omit the second order terms in our further calculations. This is justified since the maximum value of the heat capacity of a single bond is approximately in the order of k_B (Appendix A) per degree of freedom. This quantity can never be bigger than the enthalpic contribution in this term. This is still true if we imagine a situation where the bond will be described by more degrees of freedom (such as ten, which is approximately the maximal number of degrees of freedom for a single bond between two monomeric units).

For simplicity, we will work out a case in which we expand K_a up until zeroth order and all elongation constants to first order. For the moment, we assume that the ratio of elongation constants at the polymerization temperature are approximately equal, i.e., $\kappa_{BA}^* \simeq 1$. In Chapter 3, we shall see that small deviations from this value will greatly improve the quality of the experimental data fits. We then find for δ,

$$\delta = \frac{h_{e,A}^* - h_{e,B}^*}{k_B T_p}\left(\frac{T}{T_p}-1\right), \tag{2.30}$$

while for Y we find,

$$Y = \left[\exp\left(\frac{h_{e,A}^*}{k_B T_p}\left(\frac{T}{T_p}-1\right)\right) - 1\right] K_a^{*-1}. \tag{2.31}$$

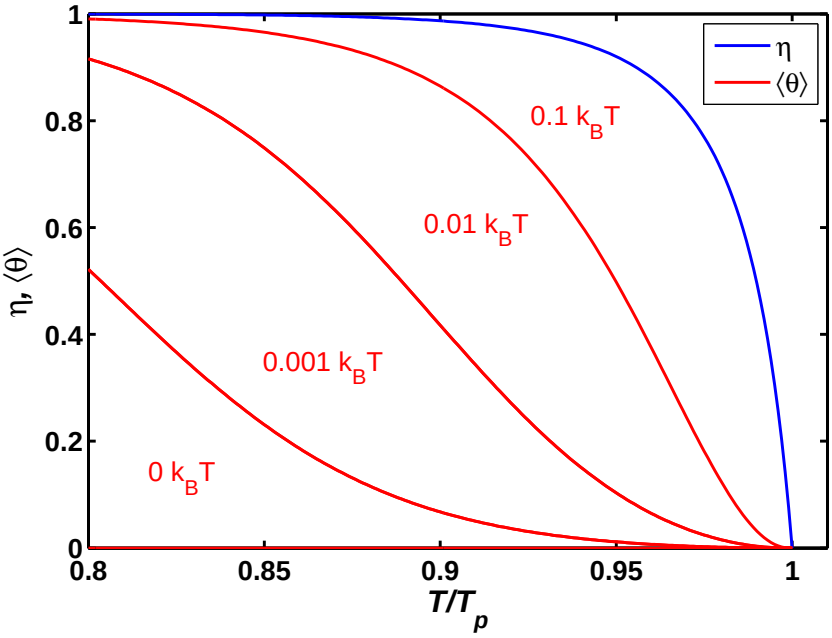

Figure 2.4: Plot of $\langle\theta\rangle$ and η as function of temperature for $K_a^* = 10^{-4}$ and enthalpy of elongation for active species A, $h_{e,A}^* = -40\ k_B T_p$. The energies written by the red curves denote the elongation enthalpy difference between active species B and A. As can be seen, only small enthalpy differences are needed for a significant net helicity. This enthalpy difference also influence the fraction polymerized material slightly, but this effect is not shown for sake of clarity.

Using these results, we have plotted the net helicity and fraction polymerized material for a fixed value for the enthalpy of elongation $h_{e,A}^*$, fixed K_a^* and for various enthalpy of elongation differences, $h_{e,B}^* - h_{e,A}^*$, in Figure 2.4 as a function of temperature. These enthalpy differences have also a small influence on the quantity η. This is not shown for the sake of clarity, since this effect is not that pronounced.

As can be seen in Figure 2.4, small enthalpy differences result in significant effects. An observable net helicity is observed even for an enthalpy difference of 0.001 $k_B T_p$. We can obtain this theoretical result, since all these small enthalpy contributions add up to result in macroscopic observables, such as a net helicity. This was also pointed out by Green and coworkers [9].

We conclude this section with a comparison of the analytical result for the net helicity and fraction polymerized material with the numerical result of a fixed point iterative method (Appendix B). A comparison can be found in Figure B.2. As can be seen, we observe deviations from this result at low temperatures. This is observed since higher order terms in δ become more important, since some of these terms will be amplified considerably by the quantity $\overline{N}_A$, which becomes very large at low temperatures.

2.5 Length distributions

In this section, we will construct expressions for the mole fractions of the various species. First, we will consider the mole fraction of inactive species. As was derived in section 2.1 from a free energy minimalization, we know that this mole fraction is equal to the fugacity λ. Furthermore, by using the definition of Λ_α and expression (2.11) we can express the mole fraction of inactive species as,

$$\phi_i = \left(1 - \frac{1}{\overline{N}_A}\right) \frac{Z_i}{Z_A} \exp(\beta G_A). \tag{2.32}$$

Note that we have again taken $\alpha = A$ as our reference state. To make use of the numerical solutions generated in the previous sections, we have to expand the activation constant to zeroth order and elongation constant to first order. The result is,

$$\phi_i = \left(1 - \frac{1}{\overline{N}_A}\right) K_a^{*-1} K_{e,A}^{*-1} \exp\left(\frac{-h_{e,A}^*}{k_B T_p}\left(\frac{T}{T_p} - 1\right)\right). \tag{2.33}$$

The same reasoning can be done for the mole fraction of active species, $\alpha = A, B$, with length N,

$$\phi_\alpha(N) = N\left(1 - \frac{1}{\overline{N}_\alpha}\right)^N \exp(\beta G_\alpha). \tag{2.34}$$

By expanding up until first order we find,

$$\phi_\alpha(N) = N\left(1 - \frac{1}{\overline{N}_\alpha}\right)^N K_{e,A}^{*-1} \exp\left(\frac{-h_{e,\alpha}^*}{k_B T_p}\left(\frac{T}{T_*} - 1\right)\right). \tag{2.35}$$

Furthermore, note that we can define the free monomer mole fraction as the sum of inactive species and active species of length $N = 1$,

$$\phi_{mon} = \phi_i + \sum_{\alpha=A,B} \phi_\alpha(1). \tag{2.36}$$

In Figure 2.5 the length distribution for $T/T_p = 0.8$ is plotted. As can be seen, a co-operativity of $K_a = 10^{-4}$ results in a mean length of the aggregates of approximately 5000. This number corresponds to the length estimated for BTAs [14] that also self-assemble in a co-operative fashion. Furthermore, we expect that a decrease in temperature results in a decrease of the mole fraction of free monomers. The free monomers are then converted in active species with length N. The mole fractions of the inactive species and active species as a function of temperature are shown in Appendix D.

To conclude this section, we discuss the influence of co-operativity on the width of the mole fraction distribution. For this purpose, we introduce the notion of a polydispersity index (PDI), defined as,

$$PDI := \frac{\sum_{N=1}^\infty N^2 \rho_\alpha \upsilon / \sum_{N=1}^\infty N^2 \rho_\alpha \upsilon}{\sum_{N=1}^\infty N \rho_\alpha \upsilon / \sum_{N=1}^\infty \rho_\alpha \upsilon} = 2 - \frac{1}{\overline{N}_A}. \tag{2.37}$$

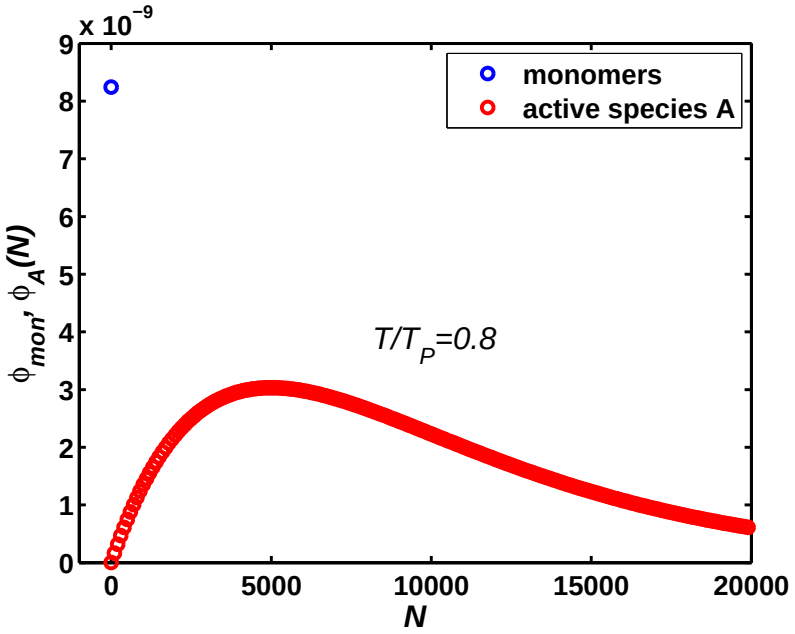

Figure 2.5: Length distributions for the monomers and active species A. In the case of $\phi_A(N)$, the active species with length $N = 1$ are excluded, since they are already included in the definition of the mole fraction of monomers ϕ_{mon}. The plot is made for $K_a = 10^{-4}$ and $h^*_{e,A} = -40\ k_BT_p$. For the elongation constant as defined on T_p, we have chosen a value corresponding to a free energy of binding of $-20\ k_BT_p$.

Note that the inactive species are not included in this definition. The PDI is a measure for the width of the distribution. The length distribution is narrow if the PDI is close to unity. In contrast, if this value approaches $PDI = 2$, we get a wider range of stack lengths present in solution. We calculate the PDI for two different values of K_a at $T/T_p = 0.95$, $h^*_{e,A} = -40\ k_BT_p$, $h^*_{e,B} = -39.95\ k_BT_p$ and $K^*_{e,A} = \ln 20$. For $K_a = 10^{-3}$, we find $PDI = 1.989$ and $\langle N\rangle = 5000$. For $K_a = 10^{-4}$, we find $PDI = 1.996$ and $\langle N\rangle = 5100$. These calculation show that mole fraction distributions are very similar in shape for various values of K_a in the nucleated case. Eventually, for low temperatures the PDI will approach a value of two. Finally, we note that K_a regulates the amount of inactive material.

Chapter 3

Comparison with experiment and experimental results

3.1 Comparison with experiments in dodecane

As mentioned in the introduction, the main goal of the model was to be able to predict self-assembly properties of the D-BTA in dilute solutions. In this section, we try to fit the data obtained from [10] in dodecane with the model of Chapter 2. Before we begin to attempt this, we have to interpret the experimental data. In the case of the UV-VIS cooling curve, we have to take into account that the baseline is non-linear. In practice, this means that we will subtract a linear baseline from the whole cooling curve, such that the values in the molecularly dissolved regime are constant and equal to zero (as we should expect). Furthermore, the data has been normalized such that the highest value is unity. In the case of the data obtained from CD spectroscopy, the data has been normalized in two ways. In the first case, we have normalized it such that the maximum value is 0.35. A motivation for this choice is given by the experiment in Figure 1.8, which argues that not all aggregates are in the same helicity at low temperatures. In the second case, we have normalized the data such that it saturates at a value of unity. It is thus assumed that the system achieves a homochiral state at sufficient low temperatures.

Table 3.1: Thermodynamic parameters obtained by fits of the UV-VIS and CD data of the D-BTA in dodecane at a concentration of $5 \cdot 10^{-5}$M and $T_p = 352$ K.

$\langle\theta\rangle_{\text{sat}}$	K_a	$\log_{10}\kappa^*_{BA}$	$h^*_{e,A}[J]$	$h^*_{e,A} - h^*_{e,B}[J]$
0.35	$(7 \pm 1) \cdot 10^{-4}$	-0.0014 ± 0.003	$(-18 \pm 1)\ k_B T_p$	$(-0.005 \pm 0.002)\ k_B T_p$
1.00	$(7 \pm 1) \cdot 10^{-4}$	-0.0035 ± 0.0005	$(-21 \pm 1)\ k_B T_p$	$(-0.05 \pm 0.01)\ k_B T_p$

In Figure 3.1 and Table 3.1 the results of the fits are shown. The fits were obtained by using the numerical methodology of Appendix B. The results are governed by the parameters $h^*_{e,A}$, $h^*_{e,B}$, K^*_a and κ^*_{BA}. We have chosen to let κ^*_{BA} deviate from one (Table 3.1), since this will dramatically increase the quality of the fits. It results in a

sharper transition from a regime in which $\langle\theta\rangle = 0$ to a regime of non-zero net helicity. Interestingly, only small deviations from one are enough.

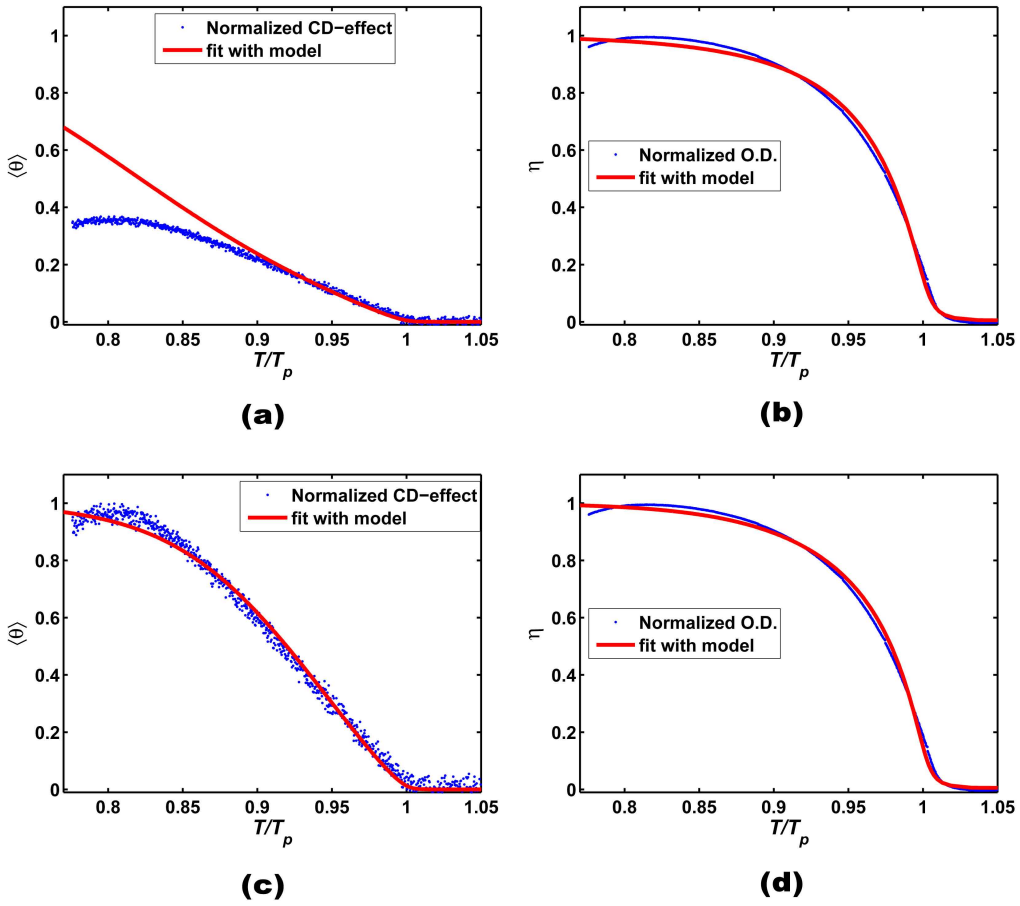

Figure 3.1: Fits obtained by the competing nucleated self-assembly model for (a) a net helicity normalized on 0.35 and (b) fraction polymerized material normalized on unity. Also the results are shown for (c) net helicity normalized on unity and (d) fraction polymerized material normalized on unity. The experimental data is obtained from a dodecane solution of the D-BTA at a concentration of $5 \cdot 10^{-5}$ M. [10]

The results of the first case are shown in the Figures 3.1(a) and 3.1(b). As can be seen, a fit of the net helicity is only possible at high temperatures, while a clear deviation is seen at low temperatures. Low enthalpy differences are needed to achieve this. The difference of the enthalpy of elongation of species B and A is only 0.005 $k_B T_p$, while $\kappa^*_{BA} \simeq 0.997$. Moreover, we see that the UV-data appears to have a small maximum at low temperatures. This may be the caused by the nonlinear baseline as discussed in Chapter 1. It is difficult to correct for this effect. As a final remark, we obtain a value of the activation constant that is slightly higher than for the achiral BTA [14].

The fits where we have allowed the existence of a homochiral state are seen in Figures 3.1(c) and 3.1(d). A very good agreement with experimental data is obtained. We notice it that is considerably better compared to Figure 3.1(a). Similarly as in the previous case, the enthalpy difference of elongation is still very small ($0.05\ k_B T_p$) and there is only a small preference for B over A at the polymerization temperature, given by $\kappa^*_{BA} \simeq 0.991$. However, it is still a concern why the model cannot predict a saturation value of the net helicity unequal to unity as was proposed by the experiment described in Figure 1.8.

3.2 Self-assembly of D-BTA in heptane at low temperatures

As mentioned in the first chapter, Cotton effects are solvent dependent in the case of D-BTAs. While we do observe a Cotton effect in dodecane, it is absent in bulkier solvents such as iso-octane (a branched alkane) or MCH (a cyclic alkane) at room temperature. Heptane is another solvent in which chirality is expressed by the deuterated BTAs at room temperature and is just like dodecane an linear alkane. However, as can be seen in Figure 1.7(b) extrema are observed in temperature dependent CD, which are absent in UV-VIS measurements (Figure D.1). We will have a closer look at what is physically happening at these extrema in this section. Therefore, experiments were conducted using CD and UV-VIS spectroscopy during this project, by using heptane as a solvent. For details concerning the experimental method, we refer to [12].

The result of Figure 1.7 is repeated in Figure 3.2(a), where we have zoomed in the temperature regime between -10°C and 50°C. The extrema are observed as an initial decrease of the CD effect (in absolute value) at low temperatures, followed by an increase (in absolute value). This increase even persists at temperatures lower than 0°C. To make certain that this is not due to optical effects, a detailed analysis of the shape of the Cotton effect is made for various temperature regimes, as indicated by the three colors in Figure 3.2(a). For various temperature regimes the CD spectra as function of temperature are shown. Surprisingly, we observe a change in the shape of the CD spectrum similar to the odd-even effect discussed in section 1.1. Note also that this shape change may as well affect the actual shape of the curve at temperatures lower than 0°C. However, as the change in wavelength at which the maximum Cotton effect is observed is small, we do not expect large differences between our measurements and the actual shape of the curve at the low temperature regime.

The change of the shape of the Cotton effect is gradual and occurs at the low temperature extremum, in this case around 10°C. It is exclusively observed by a change in temperature, in contrast to the odd-even effect observed with methylated BTAs (which is due to comparing different chemical structures). For this reason, we call this an odd-even *like* effect. However, we were not able to measure this effect when using dodecane as a solvent. The effect may be present, but it cannot be observed because of the high melting point of dodecane (-9.6°C). Cooling to temperatures below 0°C is thus not been performed.

Odd-even effects are usually encountered on a larger length scale, such as in liquid crystals [7]. This odd-even effect is for example observed in the transition temperature from a liquid or solid state to a liquid crystalline state. Another example is an odd-even effect in the screw sense of a cholesteric phase. Similarly to these observations, we may hypothesize that in our case somehow the solvent takes part of the supramolecular polymer. This was also already pointed out in the case of oligo(p-phenylenevinylene) derivatives [15].

We conclude this section by noting that we have not attempted to fit the experimental data in heptane, since the cooling curves are similar to the dodecane cooling curves for temperatures higher than 25°C. We believed that the model is not able to predict the maximum and minimum in CD effect at lower temperatures. However, at the end of this project, we have seen that it may be possible to predict the high temperature extremum in the net helicity. This was not investigated thoroughly, since it was beyond the scope of the project. A short description of this observation is included in Chapter 4 as an outlook.

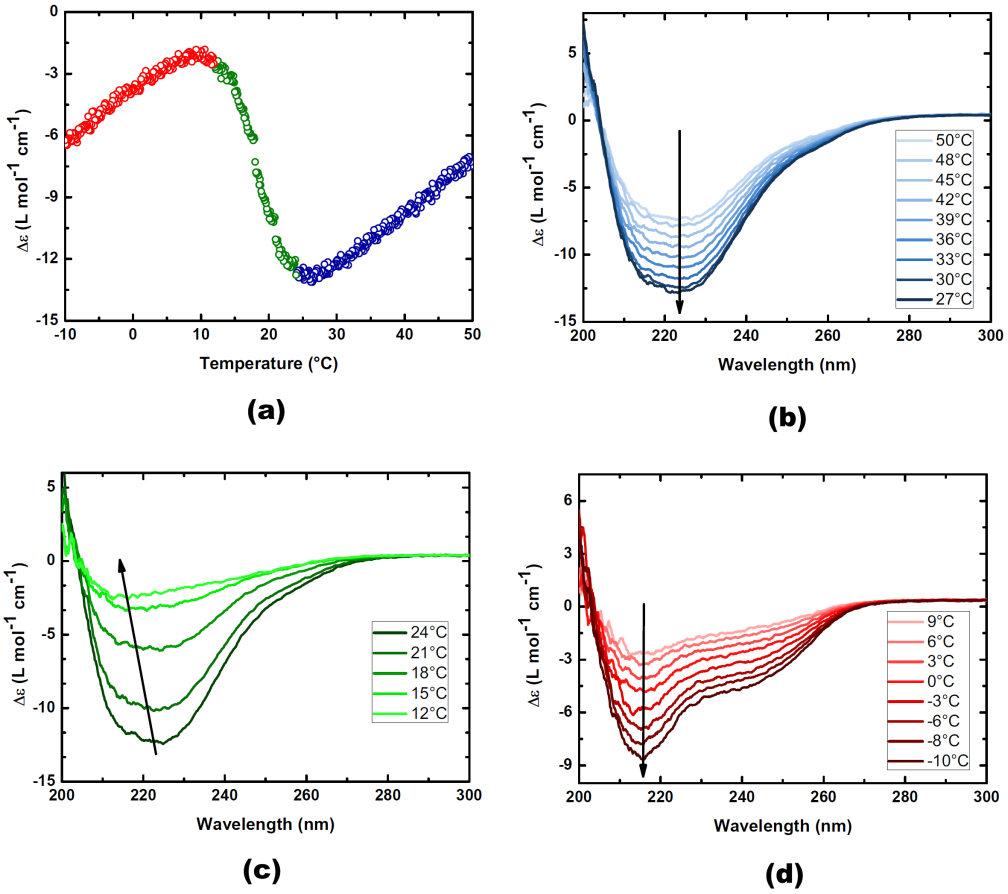

Figure 3.2: (a) Temperature dependent CD as monitored at 223 nm for (S)-D-BTA in a concentration of $5 \cdot 10^{-5}$M in heptane. A small part of the total curve is shown. The curve is divided in three parts for which the CD-spectra as function of temperature is measured for the regime (b) $27°\text{C} - 50°\text{C}$, (c) $12°\text{C} - 24°\text{C}$ and (d) $-10°\text{C} - 9°\text{C}$. In all three cases (b)-(d), the arrow indicates cooling.

Chapter 4

Conclusions and outlook

The goal of this project was to predict the net helicity and fraction polymerized material of D-BTAs in dilute solutions for a limited temperature regime. In our approach, we have used a competing nucleated self-assembly model by extending the actin polymerization model of Oosawa and Kasai. We had to limit the temperature regime, since in the solvent heptane, extrema are observed for which we believed that they could not be predicted by this hypothesis. Presumably, these extrema are present due to an active role of solvent in the self-assembly process.

Good agreements are found with the experimental data by using this model in dodecane. It was found that the difference in enthalpy of elongations between the two types of aggregates is much smaller than the unit of k_BT. The value of this difference depends on the normalization of the experimental data, and was found to be $0.05\ k_BT_P$ if the net helicity and fraction polymerized material are normalized to unity. That this could still result in macroscopic observables, such as a net helicity, is due to the fact that all these small enthalpy differences add up in an aggregate to have large effects. This is possible since the aggregates become very long, with an average of approximately 5000 monomeric units in one stack [14]. It was also observed that the ratio of elongation constants κ^*_{BA} needs to be perturbed from unity to give species A a small preference over B, to get a better agreement with experimental data. This preference is small $\kappa^*_{BA} \simeq 0.992$, but it results in a sharper transition between a regime of zero net helicity and a regime in which a net helicity can be observed. This sharp transition is also observed in our experiments. Finally, the temperature regime in which a good agreement with experimental data is found, becomes limited if we normalized the data such that the system saturates at a net helicity of 0.35.

As for a theoretical outlook on this topic, we would recommend an extension of the model by Jeroen van Gestel [16], which gives a microscopic description of a helical aggregate by using the 1D Ising model. For instance, an extension by introducing co-operativity in this model seems to be worthwhile. A microscopic description is interesting, since we cannot exclude the existence of 'mixed' aggregates, in which both P and M-helices exist in the same aggregate. Possibly, there could be a gradual transition between the P-regime to the M-regime. Such a state can be realized if the orientation of the hydrogen bonds are gradually tilted from one regime in the aggregate to the other. Solvent effects may also be included, but it has to be stressed that this will

result in more parameters. More independent experimental data are then needed to make sense out of the fits. Furthermore, these experimental techniques are also needed to get more insights in what actually happens at low temperatures in for instance a heptane solution. Finally, we have observed interesting behavior when titrating a MCH solution to a heptane solution [12], which we could not fully explain. These experiments also indicate that we need more experiments to learn more about this system. This shows that the D-BTA system is a challenging system to model. Interesting experimental techniques are for instance vibrational circular dichroism (VCD), microscopy (AFM, STM) and heat capacity measurements (microDSC).

We would like to conclude this report by noting some interesting observations during the calculations of the model. For instance, we could predict a net helicity that is weakly dependent on temperature by keeping the difference in enthalpy of elongation, $h^*_{e,A} - h^*_{e,B}$ zero, while the difference in the heat capacity of binding between species A and species B is small. This was not mentioned in the main text, but would be interesting to investigate further.

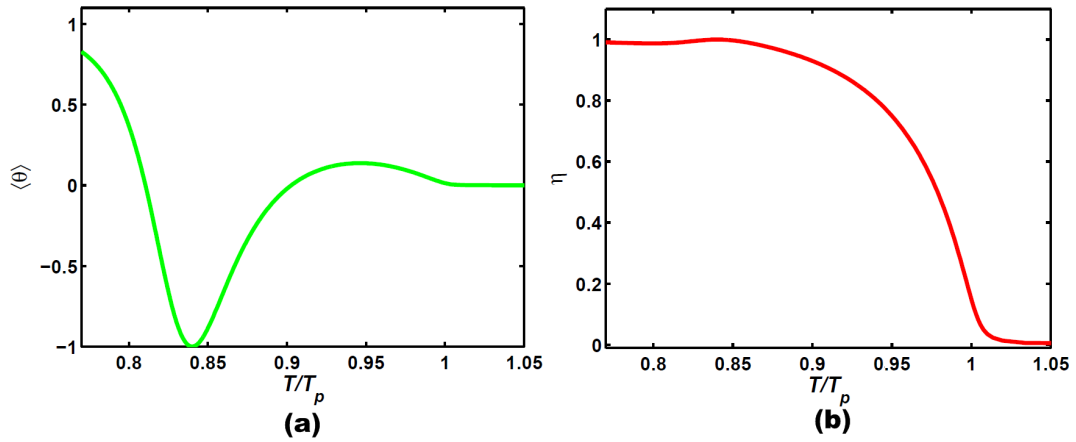

Figure 4.1: Effect of a different sign of the free energy at the polymerization temperature as compared with the difference in enthalpy of elongation, $h^*_{e,A} - h^*_{e,B}$. The curves are obtained by using the numerical methodology of Appendix B, with values for the parameters, $K^*_a = 7.5 \cdot 10^{-4}$, $h^*_{e,A} = -20\ k_B T_p$, $h^*_{e,A} = -20.09\ k_B T_p$, $\log_{10} \kappa^*_{BA} = -0.038$.

A final interesting observation is about the sign of the free energy of binding at the polymerization point, as expressed in κ^*_{BA}, compared with the sign of the enthalpy difference, $h^*_{e,A} - h^*_{e,B}$. If the signs are unequal, we are able to predict an extremum in the net helicity $\langle\theta\rangle$ and fraction polymerized material η. However, if the enthalpy difference is small, the extremum in η reduces to a 'distortion' at low temperatures (cf. Figure 4.1(b)). This is also observed in experimental data (cf. Figure D.1). In contrast, the extremum in net helicity is shifted towards lower temperature, while it is near the polymerization temperature if the enthalpy difference is large (say $> 1 k_B T$). An example of such a distortion for η and an extremum in $\langle\theta\rangle$ at low temperatures are seen in Figure 4.1. Remarkably, it is possible to obtain an extremum at a similar temperature as was measured with temperature dependent CD in heptane. This makes this observation very interesting for further research. However, since this was discovered at the end of the project (literally), we have not investigated this yet.

Acknowledgements

The following people are thanked for their help during this project: Paul van der Schoot, Anja Palmans, Seda Cantekin, Maarten Smulders, Sara Jabbari-Farouji, Patrick Stals, Hugo Meekes, Jacques van Eupen, Tom de Greef, Marko Nieuwenhuizen, Leon van Dijk, Jef Vekemans, Ronald Otten, Matthew Carnes, Thijs Michels and Bert Meijer.

Appendix A

Heat capacity of a single quantum harmonic oscillator

In this section, we will derive the heat capacity of a single quantum harmonic oscillator. This will be used as a model for a single bond between two monomeric units within a supramolecular polymer. The energy of a quantum harmonic oscillator is given by:

$$E_n = \left(n + \frac{1}{2}\right)\hbar\omega \qquad n = 0, 1, 2, ... \tag{A.1}$$

As usual $\hbar$ is the Dirac constant and ω is the angular frequency. The canonical partition function can then easily be calculated by it's definition:

$$Q := \sum_{n=0}^{\infty} \exp\left(-\beta E_n\right) = \exp\left(\frac{-\beta\hbar\omega}{2}\right) \sum_{n=0}^{\infty} \left[\exp(-\beta\hbar\omega)\right]^n \tag{A.2}$$

By noticing that we now have in fact a geometric series, we can simplify this expression by using $\sum_{n=0}^{\infty} x^n = \frac{1}{1-x}$ for which $|x| < 1$, we find for the canonical partition function:

$$Q = \frac{1}{2\sinh\left(\frac{\beta\hbar\omega}{2}\right)} \tag{A.3}$$

The heat capacity C_v can then be found by the usual recipe:

$$C_v = \frac{1}{k_B T^2} \frac{\partial^2 \ln Q}{\partial \beta^2} = k_B \left(\frac{\hbar\omega}{k_B T}\right)^2 \frac{\exp(\beta\hbar\omega)}{\left[\exp(\beta\hbar\omega) - 1\right]^2} \tag{A.4}$$

It's straightforward to see that for $T \to 0$ will result in $C_v \to 0$, while for $T \to \infty$ will result in $C_v \to k_B$. Since the heat capacity is a strictly increasing function of temperature, it's value thus varies between 0 and k_B. We can imagine that the oscillator model presented here can have many modes for the description of the bond. The above result shows that each mode will contribute a value of k_B to the value of the heat capacity in the high temperature limit. Furthermore, we can neglect the difference between C_v and C_p.

Appendix B

Numerical implementation of the model

In sections 2.2 and 2.3, we have considered the model in the long chain limit and for small perturbations for the preference of one type aggregate over the other. Of course, we can extend this notion by dropping these assumptions, but this will make finding analytical expressions for the net helicity and fraction polymerized material very difficult (if not impossible). In this case, we have to use numerical methods, for which we choose a fixed-point like iterative method. Numerical solutions that we can generate in this manner, can be applied to for instance the calculations of length distributions, for which a long chain limit is not applicable.

The starting point for our method is to start with the mass action law for two components (2.16). We do a Taylor expansion of all the elongation constants up until first order, while we do this up until zeroth order for the activation constant. The following method will not work, if we do the expansion for activation constant higher than zeroth order. The result is:

$$\exp\left(\frac{h^*_{e,A}}{k_B T_*}\left(\frac{T}{T_*}-1\right)\right) = 1 - \frac{1}{\overline{N}_A} + K_a \overline{N}_A(\overline{N}_A - 1)\left(1 + \frac{\overline{N}_B^2}{\overline{N}_A^2}\right) \tag{B.1}$$

By rewriting this expression, we can construct an iterative scheme to get the temperature T/T_* as a function of the aggregation number of species A $\overline{N}_A$.

$$\left(\frac{T}{T_*}\right)_{i+1} = 1 + \frac{k_B T_*}{h^*_{e,A}} \ln\left[1 - \frac{1}{\overline{N}_A} + K_a \overline{N}_A(\overline{N}_A - 1)\left(1 + \left(\frac{\overline{N}_B}{\overline{N}_A}\right)_i^2\right)\right] \tag{B.2}$$

Where the ratio of aggregation numbers given in the i-th iteration step is given by:

$$\left(\frac{\overline{N}_B}{\overline{N}_A}\right)_i = \left[\overline{N}_A - \exp\left(\ln \kappa^*_{BA} + \frac{h^*_{e,B} - h^*_{e,A}}{k_B T_*}\left(\left(\frac{T}{T_*}\right)_i - 1\right)\right)(\overline{N}_A - 1)\right]^{-1} \tag{B.3}$$

We go through this iteration scheme starting from $i = 1$ and as our initial value we take $\left(\overline{N}_B/\overline{N}_A\right)_1 = 1$. An implementation in MATLAB would be:

```
%Iterative process to get temperature versus aggregation number

close all;
clear all;

%Defining constants

heB = -39.995;      % Enthalpy of elongation for A given in units of kT
heA = -40;          % Enthalpy of elongation for B given in units of kT
Ka = 1*10^-4;       % Activation constant
KBA = 1             % Ratio of elongation constants
M = 20000;          % Maximal mean aggregation number for A

%Create list of values

T_Tp= zeros(N,10);

%Starting estimate (aggregation number = i+0.01)
for i = 1:N
    T_Tp(i,1) = 1+(1/heA)*log(1-1/(i+0.01)+2*Ka*(i+0.01)*((i+0.01)-1));
end


for j = 2:10
    for k = 1:M
        T_Tp(k,j) = 1+(1/heA)*log(1-1/(k+0.01)+Ka*(k+0.01)*((k+0.01)-1)+...
            Ka*((k+0.01)-exp(log(KBA)+(heB-heA)*(T_Tp(k,j-1)-1)))^-2*...
            (k+0.01)*((k+0.01)-1));
    end
end
```

Furthermore, we can make a comparison of this scheme by considering the long chain limit. In this limit, we can find an analytical expression for the reduced temperature (T/T_p) as a function of $\overline{N}_A$. By plotting the result explicitly, we can see that in the second iteration step the solution already converges. Furthermore, the behavior of the solution in the long chain limit is as to be expected (cf. Figure B.1).

Finally, we note that this script will not work for isodesmic behavior. The reason is that high temperatures cannot be achieved when $\overline{N}_A$ is used as a parameter. The reason is clear: there are no active species at temperatures higher than T_p.

As an application of this method, we can write the net helicity $\langle\theta\rangle$ and fraction polymerized material η as a function of $\overline{N}_A$. Combined with the fact that we have the temperature as a function of $\overline{N}_A$, we can plot numerical results for $\langle\theta\rangle$ and η. This can be seen in Figure B.2, with a comparison of the analytical result (section 2.3) included. The discussion for the deviation at low temperatures can be found in section 2.3.

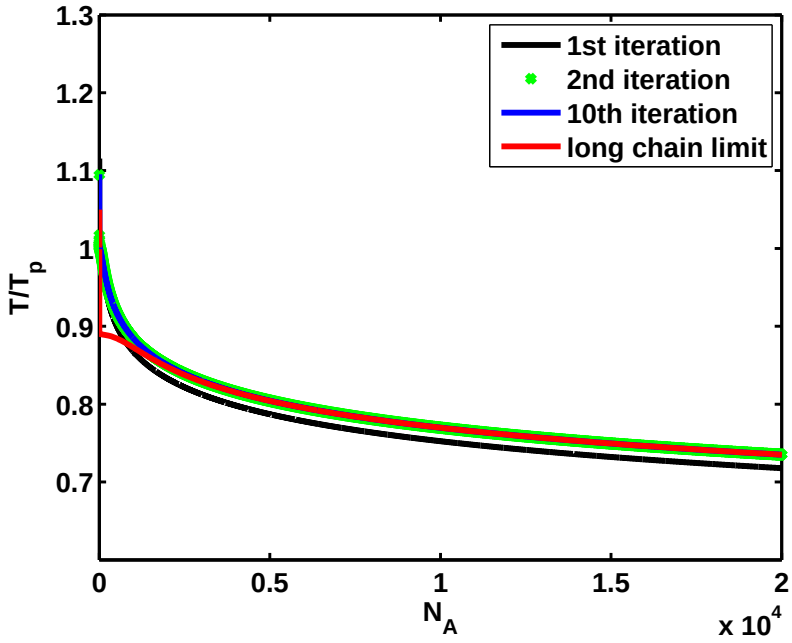

Figure B.1: Temperature obtained by a parametrization with the aggregation number $\overline{N}_A$. As can be seen already after the second iteration the solution converges. Also plotted is the long chain limit; the agreement for high $\overline{N}_A$ is very good with this analytical expression.

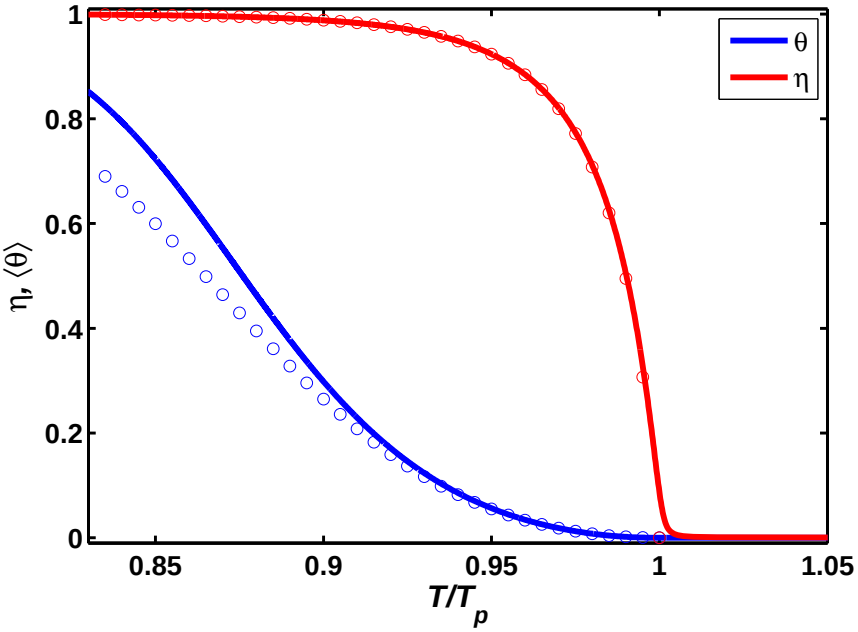

Figure B.2: Comparison between analytical solution as obtained with perturbation theory (○) with the numerical solutions by the fixed point iteration presented in this Appendix (-). The values used for these plots are $K_a^* = 10^{-4}$, $h_{e,B}^* = -39.995$ $k_B T_p$ and $h_{e,A}^* = -40$ $k_B T_p$.

Appendix C

Choice of reference volume

In the competing nucleated self-assembly model that is derived in Chapter 2, we had to use a reference volume υ to make the number density ρ_k ($k = i$, A, B) dimensionless. The choice of this reference volume is not trivial, as is discussed in [7]. Normally, this reference volume is taken as the volume of a monomeric unit. In contrast, we have chosen to take the volume of a solvent molecule as a reference in our model. Both choices will result in different interpretations of the quantities defined in equations 2.4, 2.5 and 2.6. Here, we will give a brief discussion of this interpretation.

If we choose υ to be the volume of a monomer, it implies that $\rho_k = N'_k/V$, with N'_k the number of species k and V the system volume. Filling in this expression in the definition of for instance ϕ_i will result in:

$$\phi_i := \rho_i \upsilon = \frac{N'_i \upsilon}{V} = \frac{V_i}{V} \tag{C.1}$$

Here V_i is the total volume taken in by the inactive species. The derivation in the case of active species is similar. Clearly, this indicates that for this choice ϕ_i, $\phi_\alpha(N)$, ϕ_α and ϕ represent volume fractions.

In the case that υ is a solvent molecule volume, we have $\upsilon = 1/\rho_s$, with ρ_s the number density of solvent molecules. Again using this in the definition of ϕ_i (other cases follow in the same manner), we find:

$$\phi_i := \rho_i \upsilon = \frac{\rho_i}{\rho_s} \simeq \frac{\rho_i}{\rho_s + \rho_i} = \frac{N'_i}{N'_s + N'_i} \tag{C.2}$$

We have assumed dilute conditions at the "$\simeq$"-sign and N'_s is defined as the total number of solvent species. Now we see that it represents a mole fraction. We have chosen for this definition since mole fractions are easier to interpret. Note that this choice is arbitrary.

Appendix D

Supporting figures

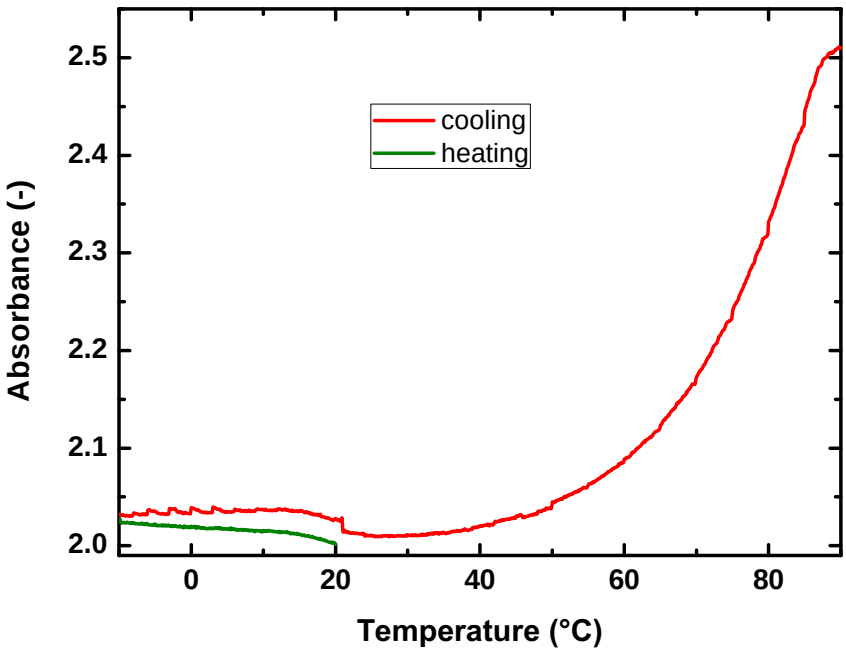

Figure D.1: Temperature dependent UV-VIS spectroscopy of a D-BTA solution in heptane ($c = 5 \cdot 10^{-5}$M), which is a measure for the fraction polymerized material η. Raw data is shown, meaning that it is not normalized and that it is not corrected for the non-linear baseline. The two extrema seen with CD spectroscopy are not observed here. Also note that subsequent heating after cooling could not reproduce the O.D. obtained earlier with cooling. There is also a small 'distortion' observed at low temperatures. The reason for this is unclear. This could be a device problem since the sample is cooled down to the limits of the temperature controller ($-10°$C). However, this distortion is also predicted by theory (see Chapter 4).

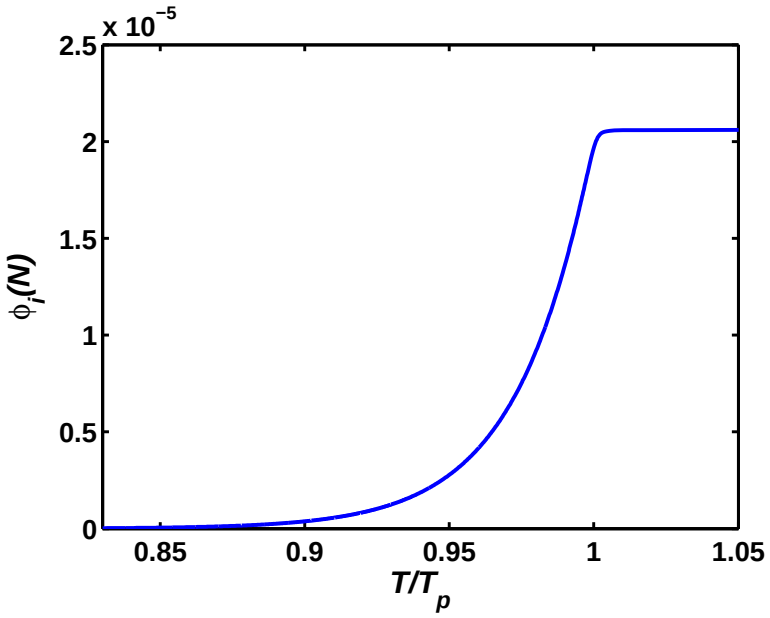

Figure D.2: The mole fraction of inactive species as a function of temperature. This curve is obtained from theory (as described in section 2.4). The curve is obtained for $K_a = 10^{-4}$, $h^*_{e,A} = -40\ k_B T_p$. For the elongation constant as defined on T_p, we have chosen a value corresponding to a free energy of binding of $-20\ k_B T_p$.

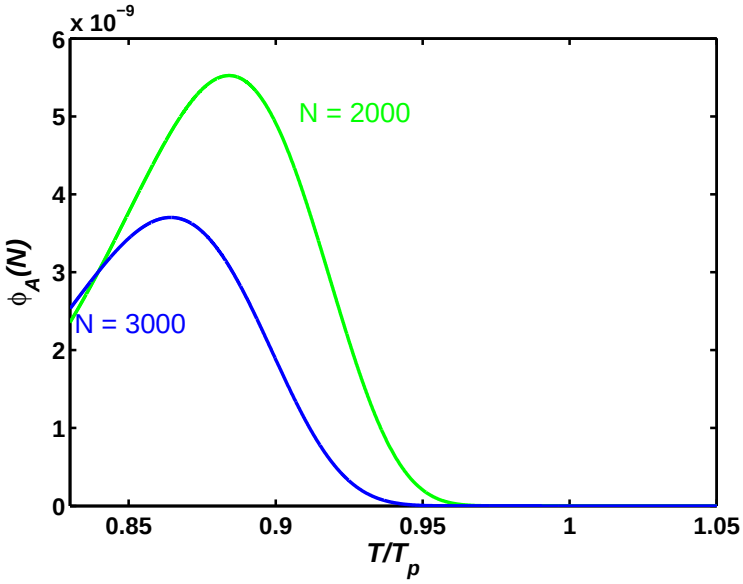

Figure D.3: The mole fraction of active species as a function of temperature for two different stack lengths N. This curve is obtained from theory (as described in section 2.4). The curve is obtained for $K_a = 10^{-4}$, $h^*_{e,A} = -40\ k_B T_p$. For the elongation constant as defined on T_p, we have chosen a value corresponding to a free energy of binding of $-20\ k_B T_p$.

Bibliography

[1] B. Alberts, A. Johnson, J. Lewis, m. Raff, K. Roberts, P. Walter, *Molecular Biology of the Cell*, 5th edition, (Garland Science, New York **2008**).

[2] J.M. Berg, J.L. Tymoczko, L. Stryer, *Biochemistry*, 6th edition, (Freeman, New York, **2007**).

[3] M. P. Lightfoot, F. S. Mair, R. G. Pritchard, J. E.Warren, *Chem. Commun.* **1999**, 1945-1946.

[4] P.J.M. Stals, M.M.J. Smulders, R. Martín-Rapun, A.R.A. Palmans, E.W.Meijer. *Chem. Eur. J.* **2009**, *15*, 2071-2080.

[5] G. Gottarelli, S. Lena, S. Masiero, S. Pieraccini, G.P. Spada, *Chirality* **2008**, *20*, 471-485.

[6] F. Oosawa, M. Kasai, *J. Mol. Biol.* **1962**, *4*, 10-21.

[7] P. van der Schoot, *Nucleation and Co-Operativity in Supramolecular Polymers* In: *Advances In Chemical Engineering Volume 35*, Academic Press, **2009**.

[8] P. van der Schoot, *Theory of Supramolecular Polymerization* In: *Supramolecular Polymers* (Ed.: A. Ciferri), 2nd edition, (Taylor and Francis, London, **2005**).

[9] K. Cheon, M.M. Green, *J. Label. Compd. Radiopharm.* **2007**, *50*, 961-966.

[10] S. Cantekin, D. Balkenende. Unpublished results concerning deuterated BTAs.

[11] M. Bellot, L. Bouteiller, *Langmuir* **2008**, *24*, 14176-14182.

[12] J.C. Everts, *Expression of chirality in deuterated benzenetricarboxamides*, Major project report, Eindhoven University of Technology, **2010**.

[13] M.M.J. Smulders, A.P.J.H. Schenning, E.W. Meijer, *J. Am. Chem. Soc.* **2008**, *130*, 606-611.

[14] M.M.J. Smulders, *Chirality in Supramolecular Polymers*, PhD Thesis, Eindhoven University of Technology, **2009**.

[15] P. Jonkheijm, P. van der Schoot, A.P.J.H. Schenning, E.W. Meijer, *Science* **2006**, *313*, 80-83.

[16] J.A.M. van Gestel, *Theory of Helical Supramolecular Polymers*, PhD Thesis, Eindhoven University of Technology, **2003**.